Spectral and up-conversion dynamics and their relationship to the laser properties of $BaYb_2F_8$:Ho^{3+}

Guy D. Gilliland and Richard C. Powell
Department of Physics, Oklahoma State University, Stillwater, Oklahoma 74078-0444

Leon Esterowitz
Naval Research Laboratory, Washington, D.C. 20375-5000

(Received 25 September 1987; revised manuscript received 7 July 1988)

The optical spectroscopic properties, energy transfer, up-conversion transitions, and lasing dynamics of $BaYb_2F_8$:Ho^{3+} crystals are reported here. The positions of the various Stark components of the different J manifolds of Ho^{3+} are identified, and the branching ratios and radiative decay rates were calculated for the Ho^{3+} levels from the Judd-Ofelt theory. The fluorescence-decay kinetics of the Ho^{3+} emission originating on the $^5F_5$ and $^5S_2$,$^5F_4$ levels and of the Yb^{3+} emission were measured and analyzed with two energy-transfer theories. These calculations show that the Ho^{3+}-Yb^{3+} interaction is greater for ions initially in the $^5F_5$ level and that the diffusion of excitation energy among Yb^{3+} ions is a thermally assisted incoherent hopping process with a diffusion constant of 1.1×10^{-10} cm^2/sec at 300 K. The kinetics of the up-conversion processes were modeled with rate equations. It was necessary to include the effects of stimulated emission at 551.5 nm and three successive energy transfers from Yb^{3+} to Ho^{3+} to adequately describe the spectral dynamics of the up-conversion. The efficiencies of the different laser transitions were found to be dependent upon the pump power used. The output of the shorter-wavelength transition (0.55 μm) increases at the expense of the longer-wavelength transition (2.9 μm) as the pump power is increased. The 2.9-μm laser action was found to have a 15% energy conversion efficiency and a slope efficiency of 4.5% when pumped at 1.047 μm.

I. INTRODUCTION

The phenomenon of "frequency up-conversion," the conversion of infrared light to visible light, has been extensively studied in systems containing rare-earth ions, and up-conversion pumping of rare-earth laser systems has been demonstrated.[1–18] This can be an important technique for switching lasing channels. Important factors in the choice of a host material which affect the efficiency of emission for this type of the up-conversion process are the ability of the host material to accept a large concentration of the optically active ions, and weak electron-phonon interaction so the radiative rates for the visible emitting states of the activator ion are large in comparison to the nonradiative rates.[15,19]

It is well known that holmium ions can produce stimulated emission at several wavelengths in the infrared portion of the spectrum [2.4,[3] 2.0,[3,4] and 2.9 μm (Refs. 5 and 6)] and also in the green region.[3] When co-doped with ytterbium, holmium can also convert infrared radiation into green emission efficiently enough for stimulated emission to occur.[1,2]

In this paper we report the results of an extensive investigation of the spectral, energy-transfer, up-conversion, and lasing properties of $BaYb_2F_8$:Ho^{3+} crystals. The energy levels and some of the relevant transitions for Ho^{3+} and Yb^{3+} are shown in Fig. 1. The results of measurements of the absorption and emission spectra at various temperatures as well as the results of a Judd-Ofelt analysis[15,20–22] are presented. The important features of two different up-conversion processes have been analyzed and related to the stimulated emission at 2.9, 2.0, and 0.55 μm.

II. EXPERIMENT

The sample used for this investigation was a single crystal of $BaYb_2F_8$ containing 7.0 at.% Ho^{3+} ions (9.0×10^{20} cm^{-3}) and 93 at.% Yb^{3+} ions (1.2×10^{22}

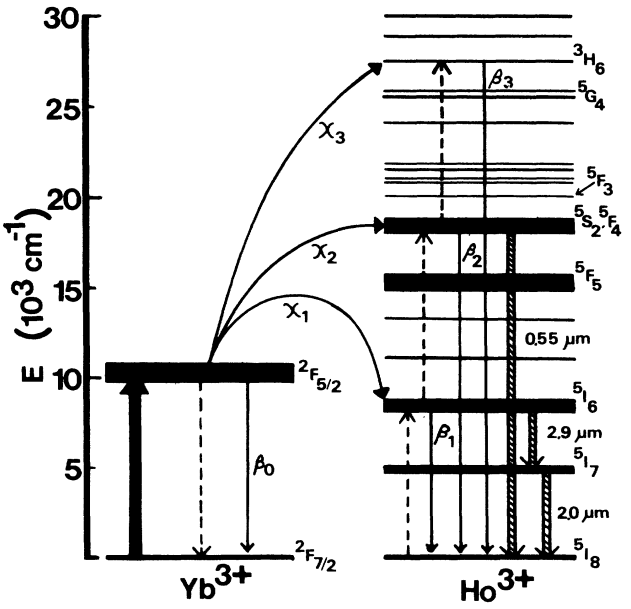

FIG. 1. Energy levels and model for up-conversion of infrared light.

cm^{-3}). It had a diameter of 5.0 mm and a length of 7.0 mm. The host crystal has the same structure as $BaTm_2F_8$, which crystallizes in the monoclinic syngony with two molecules per unit cell.[23] The space group is C_{2h}^3 (C_{2h}),[23–25] with lattice parameters $a=6.894$ Å, $b=10.53$ Å, $\zeta=4.346$ Å, and $\beta=99°18'$.[26] The Yb^{3+} ions sit in a site of eightfold coordination with F anions and form a slightly distorted Thomson cube.[25] The Ho^{3+} ions substitute for the Yb^{3+} ions. The host crystal is a single-center system, and the low symmetry of this site implies that all degeneracy in the electronic energy levels is removed except Kramers's degeneracy.[24]

The absorption and fluorescence spectra were obtained with standard spectroscopic equipment. For time-resolved energy-transfer studies, the excitation was provided by a nitrogen-laser-pumped dye laser with either Coumarin-540A or DCM dyes. For stimulated-emission measurements, the primary output from a passively mode-locked Nd:YAG (YAG denotes yttrium aluminum garnet) laser having a pulse width of 50 psec was used to pump the sample. The laser-performance measurements at 2.9 μm were done using the primary output of a Nd:YLF (YLF denotes yttrium lithium fluoride) laser at 1.047 μm with a 60-μsec pulse width as a pump source.

III. ABSORPTION AND EMISSION SPECTRA

Figure 2 shows the various regions of the absorption spectrum at 12 K. The spectrum is characterized by sharp lines in the visible region due to transitions within the $4f^{10}$ configuration of the Ho^{3+} ions, a broadband with structure in the nearinfrared due to the $^2F_{7/2}$-$^2F_{5/2}$ transition of the Yb^{3+} ions, and several absorption bands between 1.1 and 2.0 μm due to transitions to the lower-lying energy levels of the Ho^{3+} ions. Figures 3(a)–3(h) show the spectra of the visible and infrared emission of Ho^{3+} ions and the near-infrared emission of Yb^{3+} ions at 12 K. Figure 3(i) shows the 2.8-μm emission of Ho^{3+} at room temperature since it was too weak to detect at 12 K. The additional lines in the spectra at higher temperatures are due to absorption from the thermally populated higher Stark components of the $^5I_8$ ground-state multiplet of Ho^{3+}.

A comparison of the emission spectrum of Yb^{3+} at 12 K shown in Fig. 3(f) with the absorption spectrum at 12 K shown in Fig. 2(b) demonstrates that both have the same general shape. From this we conclude that the splitting of the ground-state manifold $^2F_{7/2}$ of the Yb^{3+} ions is about 760 cm^{-1}. In C_{2h} point-group symmetry each J manifold of Ho^{3+} is split by the crystal field into $2J+1$ non-Kramers levels, while each J manifold of Yb^{3+} is split into $J+\frac{1}{2}$ Kramers doublets. The crystal-field levels of Ho^{3+} have been identified from the absorption and emission spectra of $BaYb_2F_8$:Ho^{3+} and are shown in Table I. It was impossible to identify the crystal-field levels of Yb^{3+} due to the lack of resolution of the broad, overlapping levels.

The Judd-Ofelt theory[20,21] was applied to the room-temperature absorption spectrum of this sample to determine the radiative decay rates and branching ratios of the transitions. The oscillator strength of a transition of average frequency ν from a level J to the level J' is expressed as

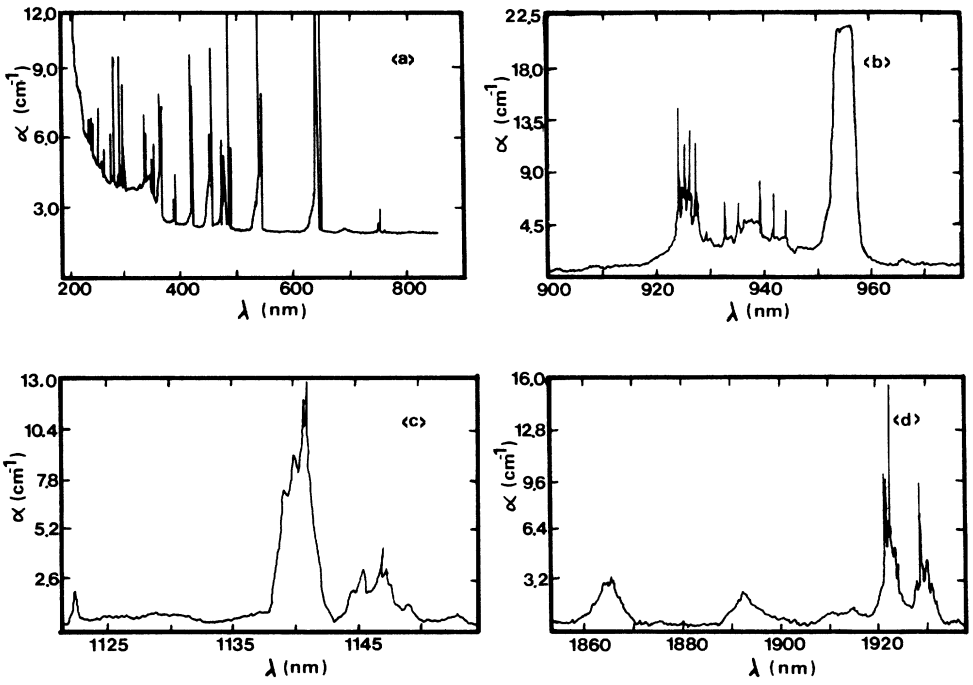

FIG. 2. Absorption spectra of $BaYb_2F_8$:Ho^{3+} at 12 K. (a) Transitions to the $^5I_4$ and higher levels of Ho^{3+}; (b) transitions to the $^2F_{5/2}$ levels of Yb^{3+}; (c) transitions to the $^5I_6$ levels of Ho^{3+}; (d) transitions to the $^5I_7$ levels of Ho^{3+}.

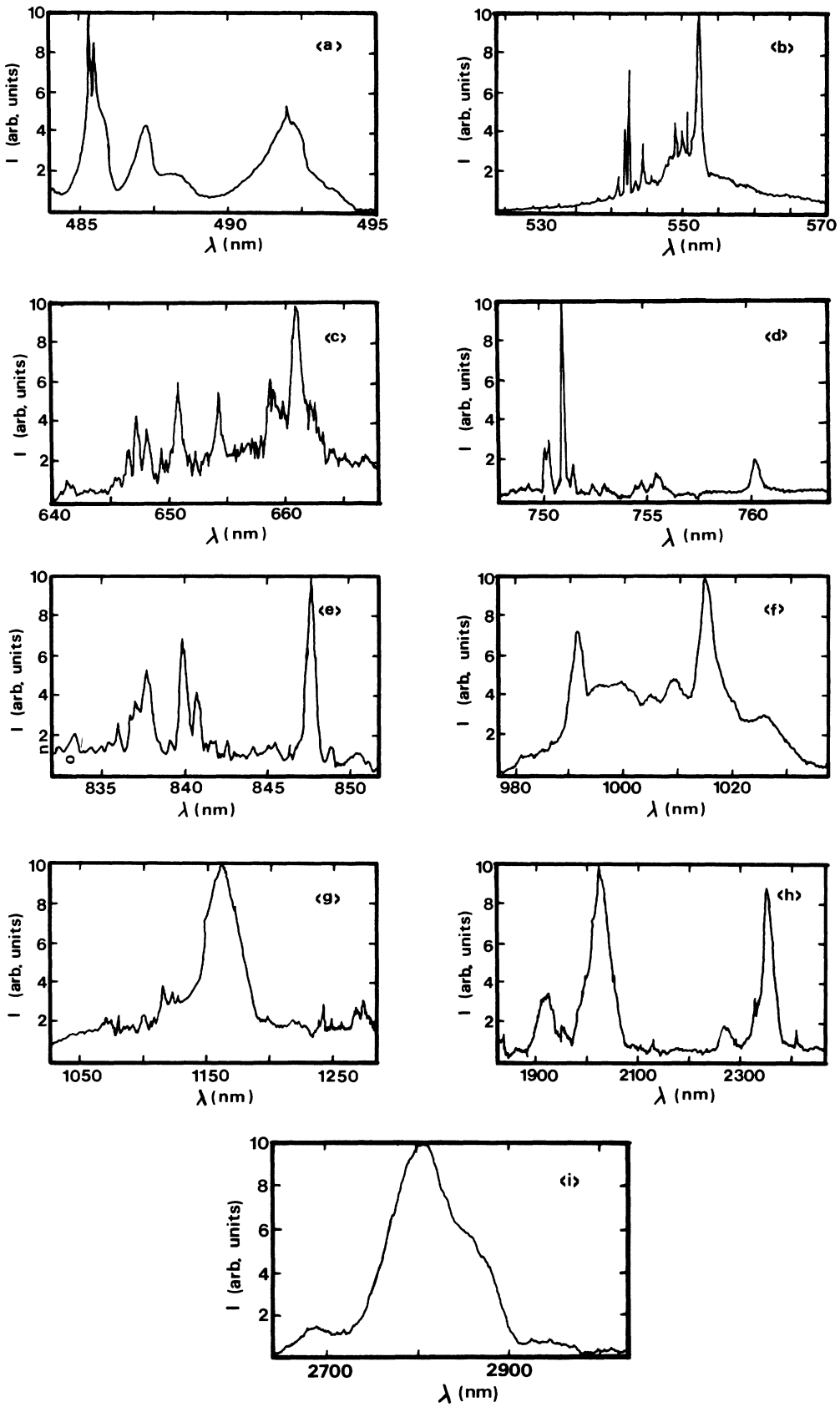

FIG. 3. Ho^{3+} and Yb^{3+} emission in $BaYb_2F_8:Ho^{3+}$: (a)–(h) at 12 K and (i) at 300 K. (a) $^5F_3$-$^5I_8$ transitions; (b) $^5S_2$,$^5F_4$-$^5I_8$ transitions; (c) $^5G_5$-$^5I_6$ transitions; (d) $^5S_2$,$^5F_4$-$^5I_7$ transitions; (e) $^5F_3$-$^5I_6$ transitions; (f) $^5S_2$,$^5F_4$-$^5I_6$ transitions; (g) $^5I_6$-$^5I_8$ transitions; (h) $^5I_7$-$^5I_8$ and $^5F_5$-$^5I_5$ transitions; (i) $^5I_6$-$^5I_7$ transitions.

$$f(aJ;bJ')=(8\pi^2 m\nu)/[3h(2J+1)e^2] \times[S_{\mathrm{ED}}(aJ;bJ')+S_{\mathrm{MD}}(aJ;bJ')] , \quad (1)$$

where the electric-dipole and magnetic-dipole line strengths are

$$S_{\mathrm{ED}}(aJ;bJ')=e^2 \sum_{t=2,4,6} \Omega_t |\langle f^n J\|U^{(t)}\|f^n J'\rangle|^2 , \quad (2a)$$

TABLE I. Energy levels of Ho^{3+} ions in $BaYb_2F_8$.

	Energy (cm^{-1})		Energy (cm^{-1})
$^5I_8$	0	$^5F_5$	15 506
	31		15 538
	45		15 545
	75		15 586
	78		15 630
	115		15 662
	125		15 696
	141		15 701
	155		15 703
	173		15 713
	205		15 715
	243	$^5S_2, ^5F_4$	18 515
	255		18 549
	270		18 560
	317		18 608
	360		18 622
$^5I_7$	5166		18 660
	5175		18 681
	5178		18 695
	5181		18 702
	5187		18 713
	5198		18 718
	5200		18 723
	5204		18 730
	5222		18 755
	5254	$^5F_3$	20 602
	5284		20 619
	5361		20 648
	5364		20 683
$^5I_6$	8673		20 734
	8703		20 747
	8713		20 777
	8716	$^3H_6$	27 563
	8719		27 609
	8731		27 655
	8736		27 732
	8764		27 778
	8767		27 840
	8773		27 871
	8779		27 933
	8910		28 011
$^5I_4$	13 221		28 121
	13 257		28 329
	13 348		28 450
	13 364		
	13 371		
	13 378		
$^5I_4$	13 380		
	13 416		
	13 514		

$$S_{\mathrm{MD}}(aJ;bJ')=[(e^2h^2)/(4m^2c^2)] \times|\langle f^n J\|L+2S\|f^n J'\rangle|^2 , \quad (2b)$$

respectively. Here, a and b represent the other quantum numbers designating the states, f^n represents the electronic configuration, $U^{(t)}$ is the tensor operator for electric-dipole transitions, $L+2S$ is the operator for magnetic-dipole transitions, and Ω_t are the phenomenological parameters associated with the crystal-field environment of the ion in the host. The reduced matrix elements in Eqs. (2a) and (2b) have been calculated elsewhere[22,27] and are essentially invariant from host to host. The oscillator strength of a transition can be calculated from the absorption spectrum at room temperature using the equation

$$f=(mcn^2)/(\pi e^2 N\chi)\int\sigma(\nu)d\nu , \quad (3)$$

where m and e are the mass and charge of the electron, c is the speed of light, N is the concentration of absorbing centers, and $\int\sigma(\nu)d\nu$ is the integrated absorption cross section. χ is the correction term for the effective field in the crystal and is approximated by $\chi_{\mathrm{ED}}=n(n^2+2)^2/9$ for electric-dipole transitions and $\chi_{\mathrm{MD}}=n^3$ for magnetic-dipole transitions where n is the refractive index of the host. Measurements of the dispersion curves have not been performed on the host at this time. A value of $n=1.6$ was used, which is similar to values of the index of refraction for other fluoride materials. It was found that varying n over a reasonable range of values did not significantly alter the results of the Judd-Ofelt analysis.

By combining Eqs. (1)–(3) and using the reduced matrix elements calculated by Weber[22] for Ho^{3+}, the phenomenological parameters Ω_t were determined from a least-squares fit to the absorption spectrum. These were found to be $\Omega_2=0.96\times10^{-20}$ cm^2, $\Omega_4=2.12\times10^{-20}$ cm^2, and $\Omega_6=3.25\times10^{-20}$ cm^2. Using these results, the spontaneous-emission probability can be obtained for each transition from

$$A(aJ;bJ')=(64\pi^4\nu^3)/[3(2J+1)hc^3] \times(\chi_{\mathrm{ED}}S_{\mathrm{ED}}+\chi_{\mathrm{MD}}S_{\mathrm{MD}}) . \quad (4)$$

The radiative lifetimes and branching ratios can be determined by

$$\tau_{Ri}^{-1}=\sum_J A(i,j) , \quad (5)$$

$$\beta(i,j)=A(i,j)/\tau_{Ri} , \quad (6)$$

where the summation is over transitions to final states j. The results of this analysis are summarized in Table II and are estimated to have an accuracy of $\pm10\%$.

IV. ENERGY-TRANSFER PROCESSES

Many theories have been developed to describe energy migration and transfer between ions. Each of these theories is limited to a specific range of parameters for which it is valid.[28–33] The results obtained in this work are analyzed with two models which are valid for

TABLE II. Radiative decay rates and branching ratios for Ho^{3+} transitions in $BaYb_2F_8$:Ho^{3+} crystals.[a]

Initial level	Terminal level	$A(i,j)$ (sec^{-1})	$\beta(i,j)$	τ_R
$^5I_7$	$^5I_8$	120.44	1.00	8.3 msec
$^5I_6$	$^5I_7$	25.87	0.09	3.5 msec
	$^5I_8$	262.63	0.91	
$^5I_5$	$^5I_6$	7.32	0.035	4.7 msec
	$^5I_7$	122.15	0.579	
	$^5I_8$	81.50	0.386	
$^5I_4$	$^5I_5$	4.52	0.044	9.7 msec
	$^5I_6$	38.77	0.376	
	$^5I_7$	49.65	0.481	
	$^5I_8$	10.30	0.099	
$^5F_5$	$^5I_4$	0.055	2.43×10^{-5}	422 μsec
	$^5I_5$	8.31	0.0037	
	$^5I_6$	110.48	0.049	
	$^5I_7$	429.39	0.190	
	$^5I_8$	1818.20	0.757	
$^5S_2, ^5F_4$	$^5F_5$	2.13	0.0004	190 μsec
	$^5I_4$	48.70	0.009	
	$^5I_5$	146.70	0.028	
	$^5I_6$	283.67	0.054	
	$^5I_7$	800.35	0.152	
	$^5I_8$	3981.90	0.756	

[a] $\Omega_2=0.96\times10^{-20}$ cm^2; $\Omega_4=2.12\times10^{-20}$ cm^2; $\Omega_6=3.25\times10^{-20}$ cm^2.

different circumstances. The Ho^{3+}-Yb^{3+} energy transfer is consistent with a single-step process while the Yb^{3+}-Ho^{3+} energy transfer is consistent with a model in which energy transfer between sensitizer and activator ions acts as a weak perturbation on the strong diffusion among sensitizers.

The typical ion-ion interaction mechanisms involving rare-earth ions are the electric multipolar mechanisms.[30,31] The strength of the interaction depends on the distance between sensitizer and activator ions as R^{-s}, where $s=6$, 8, or 10 for dipole-dipole, dipole-quadrupole, and quadrupole-quadrupole interactions, respectively. Inokuti and Hirayama have derived an expression for the time dependence of the sensitizer fluorescence in the presence of energy transfer to randomly distributed activator ions,[28]

$$I(t)=A\exp[-t/\tau-\Gamma(1-3/s)C/C_0(t/\tau)^{3/2}]\ , \tag{7}$$

where τ is the intrinsic lifetime of the sensitizer in the absence of activator ions, C is the concentration of activators, C_0 is called the "critical transfer concentration," Γ is the gamma function, and A is a normalization constant. The critical transfer distance R_0 can be determined from C_0 by[30,31]

$$R_0=(3/4\pi C_0)^{1/3}\ . \tag{8}$$

A. Ho^{3+}-Yb^{3+} energy transfer

As a first approximation, we assume that the excitation energy residing on the Ho^{3+} ions does not migrate between Ho^{3+} ions, but is capable of being transferred to Yb^{3+} ions. Thus for this case the Ho^{3+} ions play the role of sensitizer ions while Yb^{3+} ions play the role of activator ions. Justification for the assumption of no Ho^{3+}-Ho^{3+} interaction is based on the relative concentrations of sensitizer and activator ions. Because Yb^{3+} is a stoichiometric component of $BaYb_2F_8$ and there are approximately ten Yb^{3+} ions for every Ho^{3+} ion, the nearest-neighbor environment of optically active ions surrounding the Ho^{3+} ions consists almost completely of Yb^{3+} ions (assuming no clustering of Ho^{3+} ions). The Ho^{3+}-Yb^{3+} energy transfer can involve two sets of electronic-emission transitions, $^5S_2, ^5F_4 \rightarrow {}^5I_6$ and $^5F_5 \rightarrow {}^5I_7$, which are both resonant with the $^2F_{7/2} \rightarrow {}^2F_{5/2}$ absorption transition of Yb^{3+}. Therefore, the branching ratios for each of these transitions need to be considered to determine the effects of competing processes. If the Ho^{3+}-Ho^{3+} interaction is present, it will involve resonant emission and absorption transitions between the excited state, $^5S_2, ^5F_4$ or $^5F_5$, and the ground state, $^5I_8$, of Ho^{3+}. By assuming only nearest-neighbor interactions and using the branching ratios listed in Table II, we estimate that the Ho^{3+}-Yb^{3+} interaction is 3.3 times more probable than the Ho^{3+}-Ho^{3+} interaction for ions in the $^5F_5$ state of Ho^{3+} (see Fig. 4), and in the case of ions in the $^5S_2, ^5F_4$ states it is 1.1 times as probable. For randomly distributed Ho^{3+} ions the Ho^{3+}-Ho^{3+} interaction would be over distances much greater than nearest-neighbor separations and thus the interaction strength will be significantly less than the estimates given above. Therefore, the Ho^{3+}-Yb^{3+} interaction strength is greater than the Ho^{3+}-Ho^{3+} interaction strength, and as a first approximation, the theory of Inokuti and Hirayama can be used to characterize this case.

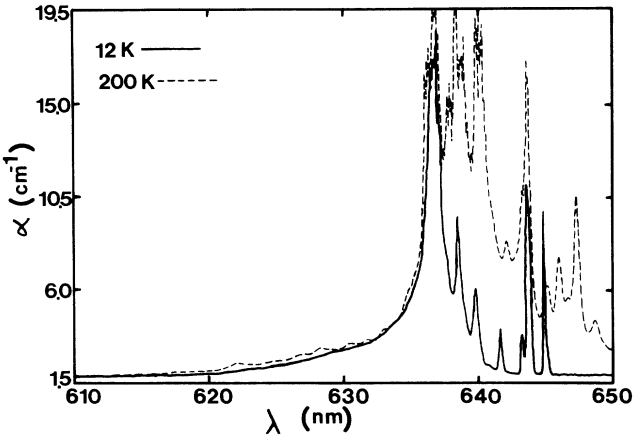

FIG. 4. Comparison of the absorption spectra at 12 and 200 K for the $^5F_5$ level of Ho^{3+}.

To characterize the energy-transfer processes, the kinetics of the fluorescence transitions between the initially excited states and the ground state of the Ho^{3+} ions was monitored. The fluorescence decay from the $^5S_2,^5F_4$ levels of Ho^{3+} was measured by monitoring the transitions terminating on the ground state at several temperatures ranging from 12 to 300 K. Figure 5 shows the decay of the fluorescence intensity at 12 K along with least-squares fits to the data using Eq. (7) for different multipolar interactions. The best fit for all temperatures is for the dipole-dipole interaction. The decay curves are all clearly nonexponential at short times for all temperatures and tend asymptotically toward an exponential at long times. The intrinsic decay rate of the Ho^{3+} ions was determined from the exponential part of the decay curves approached at long times. The theoretical curves generated from Eq. (7) were fitted to the data by treating C/C_0 as an adjustable parameter for each type of interaction ($s=6$, 8, or 10), and values for R_0 were determined using Eq. (8). The temperature dependence of R_0 for these initial conditions is plotted in Fig. 6.

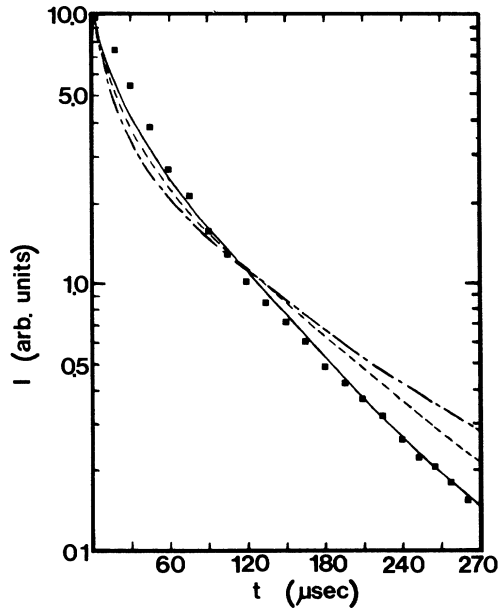

FIG. 5. $^5S_2,^5F_4$ emission at 12 K (dots), along with theoretical fits from Inokuti-Hirayama theory ($s=6$, solid line; $s=8$, short-dashed line; $s=10$, long-dashed line).

The coupling between the Ho^{3+} and Yb^{3+} ions with the former initially in the $^5F_5$ state was also investigated using Eq. (7) to fit the fluorescence-decay curves. The intrinsic decay rate in this case was again determined from the exponential tail of the decay kinetics and was found to be in substantial agreement with the measured value obtained in a sample of BaY_2F_8:Ho^{3+} which contains no Yb^{3+}.[24] The interaction mechanism in this case was again found to be electric-dipole–dipole. However, the strength of the interaction, as well as its temperature dependence, is different. The strength of the interaction, which is reflected in the magnitude of the critical interaction distance R_0, is shown as a function of temperature in Fig. 6.

Examination of Fig. 6 shows that the interaction strength between Ho^{3+} and Yb^{3+} ions is slightly greater when the Ho^{3+} ions are in the $^5F_5$ excited state than when they are in the $^5S_2,^5F_4$ excited state. The value of R_0 for the former case is close to the nearest-neighbor distance between Ho^{3+} and Yb^{3+} ions, which is approximately 2.7 Å, whereas the value of R_0 is slightly smaller than this for ions in the $^5S_2,^5F_4$ states. If the Ho^{3+} ions are directly excited, the temperature dependence of the interaction strength can affect the temperature dependence of the integrated fluorescence intensity of the Yb^{3+} ions. Figure 7 shows the temperature dependence of the integrated fluorescence intensity at 1.0 μm due to Yb^{3+} emission after two types of excitation. After pumping the $^5F_5$ state of Ho^{3+}, the interaction strength is independent of temperature and the Yb^{3+} fluorescence decreases monotonically with temperature due to some quenching mechanism in the Yb^{3+} ion, possibly energy transfer to the $^5I_6$ state of Ho^{3+}. The situation is quite different in the case of excitation into the $^5S_2,^5F_4$ states of Ho^{3+}. The temperature dependence of the Yb^{3+} emission for this case increases to a maximum at approximately 50 K and then decreases. The interaction strength depicted in

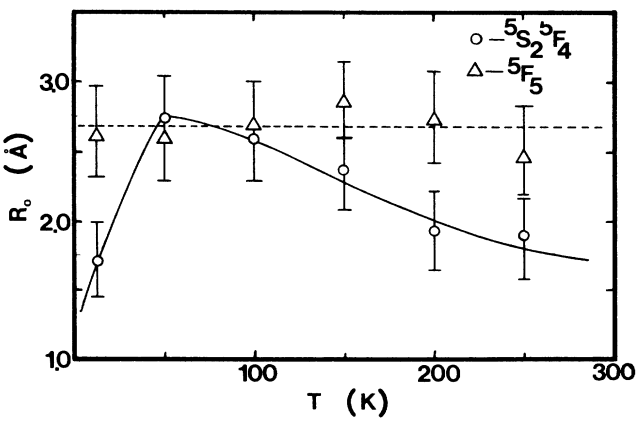

FIG. 6. Temperature dependence of R_0 for $^5F_5$ and $^5S_2,^5F_4$ states calculated from Inokuti-Hirayama theory.

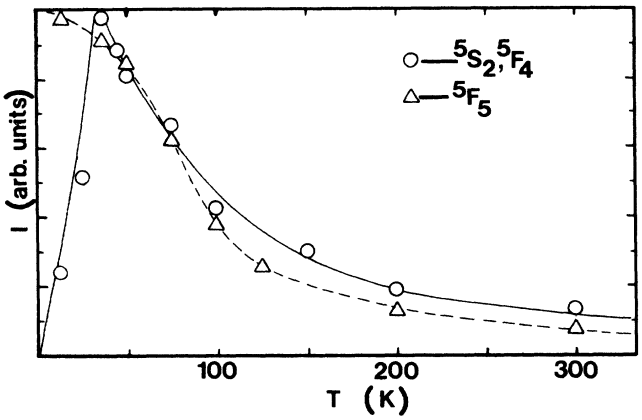

FIG. 7. Temperature dependence of integrated Yb^{3+} emission for $^5F_5$ and $^5S_2, ^5F_4$ excitation.

Fig. 6 shows the same type of temperature dependence for this excitation. Thus the increase in the fluorescence intensity at 1.0 μm up to 50 K is due to the increase in the interaction strength between the Ho^{3+} and Yb^{3+} ions, and the decrease in the fluorescence intensity above 50 K is due to both the decrease in the interaction strength and the quenching of the Yb^{3+} emission mentioned above.

B. Yb^{3+}-Ho^{3+} energy transfer

Because of the large concentration of Yb^{3+} ions, 93 at. %, when the Yb^{3+} ions play the role of sensitizers the multistep diffusion among sensitizers is dominant over the single-step direct transfer from an excited Yb^{3+} ion to an unexcited Ho^{3+} ion. For weak diffusion the theory of Yokota and Tanimoto[17,33–35] describes the energy-transfer kinetics, while for strong diffusion the theory developed by Chow and Powell[29] gives the appropriate description. Both theories were fitted to the data obtained here and it was found that the parameters describing the energy transfer are consistent with the strong-diffusion model.

The equation governing the excited sensitizer concentration $n(r,t)$ is[29]

$$\frac{\partial n(r,t)}{\partial t} = -\beta n(r,t) + D\nabla^2 n(r,t) - \sum_i v(r-R_i)n(r,t) \ . \tag{9}$$

Here, β is the intrinsic decay rate of the sensitizer ions, D is the diffusion coefficient describing the energy migration among the sensitizer ions, R_i is the position vector for a given activator ion, r is the position vector for the sensitizer ions, and $v(r-R_i)$ is the interaction strength for a given sensitizer-activator pair. The second term on the right-hand side of Eq. (9) describes diffusion among the sensitizers, while the third term describes the sensitizer-activator interaction. The solution of Eq. (9) was obtained by Chow and Powell for a dipole-dipole interaction, where $v(r-R_i)=\alpha/|r-R_i|^6$, which is weaker than energy transfer by diffusive migration. The solution of Eq. (9) was then averaged over a uniformly random activator distribution. Most theories, including this one, assume a uniformly distributed lattice of sensitizers, so that a single average hopping time can be used to describe the random walk of the excitation energy, "exciton." This situation should be valid for the "host-sensitized" energy transfer in this crystal.

The intensity of sensitizer fluorescence given by Chow and Powell is[29]

$$I_s(t) = A \exp[-t/\tau - w_{sa}(t)t] \ , \tag{10}$$

where the energy-transfer rate is given by

$$w_{sa}(t) = 4\pi D a n_a [1 + a(\pi Dt)^{-1/2}] + (4\pi n_a \alpha)/(3a^3) + 2\pi n_a a^2 \int_a^\infty dr(\alpha/r^6)\{\mathrm{erfc}[(r-a)/\sqrt{4Dt}\,]\}^2 - 8\pi n_a a \int_a^\infty dr(\alpha/r^5)\{\mathrm{erfc}[(r-a)/\sqrt{4Dt}\,]\} \ . \tag{11}$$

Here, a is the activator trapping radius, and the lower limits of the integrals do not extend to zero due to the finite nearest-neighbor distance between the sensitizer and activators. The relation between α and R_0 is

$$R_0 = (\alpha\tau_s)^{1/6} \ , \tag{12}$$

where τ_s is the intrinsic decay time of the sensitizer. The integrals appearing in Eq. (11) were evaluated numerically and the sensitizer-activator interaction constant α, diffusion coefficient D, and trapping radius a were determined by performing a nonlinear least-squares fit to the data. The intrinsic decay time of the $^2F_{5/2}$ Yb^{3+} emission has been determined previously to be 1.8 msec,[34] independent of temperature. For each set of data the validity of the Chow-Powell theory was examined. The assumptions made in deriving Eq. (10) lead to the condition[29] $\pi D a^4 \alpha^{-1} > 1$. This restriction was found to be valid for every set of data examined, typically giving a value of 31.8 for the left-hand side of the inequality. An example of the best fit to the decay kinetics of Yb^{3+} emission at 12 K is shown in Fig. 8.

The temperature dependencies of the diffusion constant D and sensitizer-activator interaction strength α obtained from the Chow-Powell theory are shown in Fig. 9. The diffusion constant increases with temperature and is 1.1×10^{-10} cm^2/sec at one. The long lifetime of $^5I_6$, 4 msec, ensures that there is sufficient population in this state for the resonant cross-relaxation process from Yb^{3+} to Ho^{3+} to occur on the time scale of the Yb^{3+} emission.

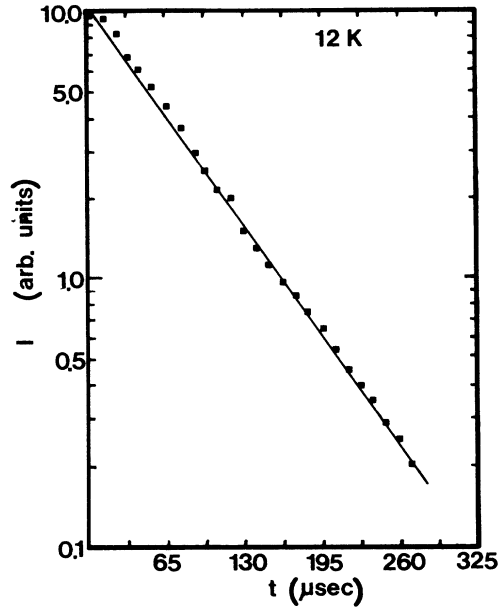

FIG. 8. Yb^{3+} emission with Chow-Powell fit (solid line) at 12 K.

V. UP-CONVERSION AND STIMULATED-EMISSION PROCESSES

Materials containing both Yb^{3+} and Ho^{3+} ions can efficiently convert 1.0-μm radiation into visible radiation.[3,9,14,18,36–39] As can be seen from the energy-level diagram for Yb^{3+} and Ho^{3+} shown in Fig. 1, Ho^{3+} has several nearly equally spaced energy levels giving rise to transitions which are coincident in energy with the $^2F_{5/2}\rightarrow{}^2F_{7/2}$ Yb^{3+} transition near 1.0 μm. The green emission corresponding to the $^5s_2,{}^5F_4\rightarrow{}^5I_8$ transition of Ho^{3+} is seen when the sample is excited with either of two longer wavelengths as discussed below, but the mechanism for the up-conversion in each case is different.

There are several multiphoton mechanisms which can be responsible for the up-conversion.[7,8,17] One possible mechanism is the sequential absorption of two pump photons by a single ion. Another possible mechanism is the absorption of pump photons by more than one ion with the subsequent energy transfer to the emitting ion.[7,8] The following results indicate that the latter mechanism is the dominant up-conversion mechanism responsible for the green emission in $BaYb_2F_8$:Ho^{3+} for both types of excitation.

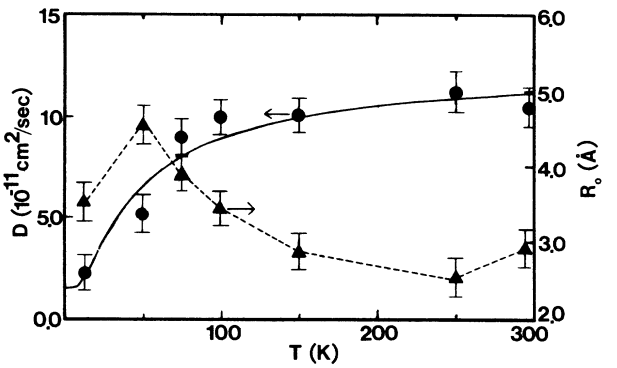

FIG. 9. Temperature dependence of diffusion constant and sensitizer-activator interaction strength calculated from Chow-Powell theory (solid line is theoretical fit for D, dashed line just shows trend of data).

The kinetics of up-conversion processes can be modeled using rate equations. The emission from $^5S_2,{}^5F_4\rightarrow{}^5I_8$ transition of Ho^{3+} after excitation into the $^5F_5$ level of Ho^{3+} state can be modeled as shown in Fig. 10. The first step in the up-conversion 300 K. The diffusion length can be determined from

$$L_d=(2D\tau)^{1/2} \tag{13}$$

and these values are listed in Table III. The accuracy of these energy-transfer parameters is estimated to be $\pm 10\%$. Figure 9 shows that the sensitizer-activator in-

TABLE III. Energy-transfer parameters.

	12 K		250 K	
	R_0 (Å)	Rate at 2.7 Å (sec^{-1})	R_0 (Å)	Rate at 2.7 Å (sec^{-1})
		$Ho^{3+}\rightarrow Yb^{3+}$ transfer		
$^5F_5$	2.6	1.3×10^4	2.3	4.9×10^3
$^5S_2,{}^5F_4$	1.7	1.0×10^3	2.1	3.0×10^3
	12 K		250 K	
		$Yb^{3+}\rightarrow Ho^{3+}$ transfer		
$D=2.1\times10^{-11}$ cm^2/sec			$D=1.5\times10^{-10}$ cm^2/sec	
$R_0=3.56$ Å (S-A)			$R_0=2.54$ Å (S-A)	
$R_0=10.3$ Å (S-S)			$R_0=13.8$ Å (S-S)	
$L_d=27.5$ Å			$L_d=84.9$ Å	
$D(0)=1.55\times10^{-11}$ cm^2/sec				
$B=1.10\times10^{-10}$ cm^2/sec				
$\Delta E=27.3$ cm^{-1}				

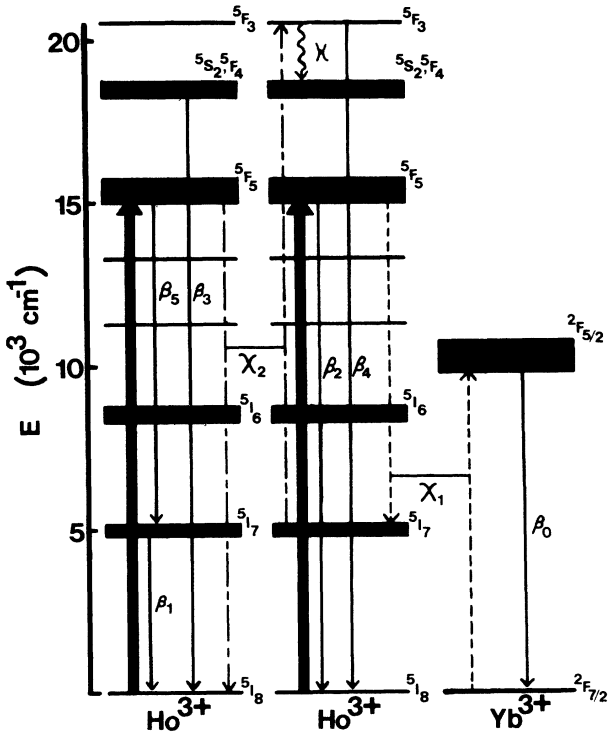

FIG. 10. Energy levels and model for up-conversion of red light.

teraction strength has the same temperature dependence as that calculated for the Ho^{3+}-Yb^{3+} transfer from the theory of Inokuti and Hirayama. The major difference is that the role of the sensitizer and activator ions are reversed in these two cases. For resonant processes the interaction strength is contained in the overlap integral between the sensitizer emission and activator absorption. The magnitude of the spectral overlap changes depending on which ion acts as sensitizer and activator due to the energy shift for emission for both Ho^{3+} and Yb^{3+} ions. However, the variation of the spectral overlap with temperature is essentially the same for both cases.

The actual measurement was performed by pumping the $^5S_2$,$^5F_4$ states of Ho^{3+} and monitoring the Yb^{3+} emission. The population of the Yb^{3+} excited state is achieved by the resonant cross-relaxation process

$$|\,Ho^{3+}(^5S_2,^5F_4),Yb^{3+}(^2F_{7/2})\rangle \rightarrow |\,Ho^{3+}(^5I_6),Yb^{3+}(^2F_{5/2})\rangle\ .$$

Initially the population of $^5I_6$ is equal to that of the $^2F_{5/2}$ state of Yb^{3+}. Therefore the energy transfer from Yb^{3+} to Ho^{3+} can take place via two types of processes. The first is transfer to the $^5I_6$ state via a phonon-assisted energy transfer. The second is the resonant cross relaxation

$$|\,Yb^{3+}(^2F_{5/2}),Ho^{3+}(^5I_6)\rangle \rightarrow |\,Yb^{3+}(^2F_{7/2}),Ho^{3+}(^5S_2,^5F_4)\rangle\ .$$

The temperature dependence and difference in rates between resonant and nonresonant processes, calculated below, point to the second mechanism as the dominant is the resonant cross-relaxation process

$$|\,Ho^{3+}(^5F_5),Yb^{3+}(^2F_{7/2})\rangle \rightarrow |\,Ho^{3+}(^5I_7),Yb^{3+}(^2F_{5/2})\rangle\ .$$

The relative probability of this process is related to the branching ratio for the Ho^{3+} transition, which is listed in Table II as 0.19. Therefore, this transition is one-fourth as probable as the transition originating from this excited level and terminating on the ground state. A rate-equation analysis of the energy-transfer rate between sensitizers and activators, when two energy levels are taken to characterize these ions, gives a relationship between the energy-transfer rate and the risetime of the activator emission[40]

$$t_{\max}=(P_A^r-P_S^r-P_{SA})^{-1}\ln[P_A^r/(P_S^r+P_A^r)] \tag{14}$$

where P_A^r and P_S^r are the radiative rates of the sensitizer and activator, respectively, and P_{SA} is the energy-transfer rate. The Yb^{3+} emission has a risetime of 4 μsec for this excitation which implies that the Ho^{3+}-Yb^{3+} transfer occurs with a rate of 1.5×10^5 sec^{-1}. Thus this first step in the up-conversion process also explains the observed Yb^{3+} emission. The second step in the up-conversion process can proceed by one of two mechanisms. The first is a resonant cross-relaxation between two Ho^{3+} ions,

$$|\,Ho^{3+}(^5F_5),Ho^{3+}(^5I_7)\rangle \rightarrow |\,Ho^{3+}(^5I_8),Ho^{3+}(^5F_3)\rangle\ ,$$

and the second is the absorption of an excitation photon by a Ho^{3+} ion that has already participated in the first step and is in the $^5I_7$ level. The last step involves both weak fluorescence from the $^5F_3$ level followed by fast nonradiative decay to the $^5S_2$,$^5F_4$ states and the green emission.

If a second cross-relaxation process is responsible for the excitation into the $^5F_3$ state, then it will originate on the $^5I_7$ level of a Ho^{3+} ion which has already undergone the first cross-relaxation process. The reason for this is that the radiative lifetime of the $^5I_7$ level is 9 msec while that of the $^5F_5$ level is 420 μsec. If a single ion were to absorb a photon, undergo cross relaxation, and then absorb another photon, it would require that the cross-relaxation process be faster than the duration of the pump pulse. This rules out the sequential two-photon mechanism because the pulse width of the laser excitation is 10 nsec, and the cross-relaxation time, reflected in the risetime of the $^2F_{5/2}$ Yb^{3+} emission, is 4 μsec at 12 K.

The rate equations used to analyze the spectral dynamics are

$$\frac{ds_1}{dt}=\chi_1 n_2(S-s_1)-\gamma_1 s_1 n_1-\beta_0 s_1\ , \tag{15a}$$

$$\frac{dn_1}{dt}=\chi_1 n_2(S-s_1)-\gamma_1 s_1 n_1-\chi_2 n_1 n_2 +\gamma_2 n_4(N-n_1-n_2-n_3-n_4)-\beta_1 n_1+\beta_5 n_2\ , \tag{15b}$$

$$\frac{dn_2}{dt}=W_p(N-n_1-n_2-n_3-n_4)-\beta_2 n_2 -\chi_1 n_2(S-s_1)+\gamma_1 s_1 n_1-\chi_2 n_2 n_2 +\gamma_2 n_4(N-n_1-n_2-n_3-n_4)-\beta_5 n_2 , \quad (15c)$$

$$\frac{dn_3}{dt}=\kappa n_4-\beta_3 n_3 , \quad (15d)$$

$$\frac{dn_4}{dt}=\chi_2 n_1 n_2-\gamma_2 n_4(N-n_1-n_2-n_3-n_4) -(\kappa+\beta_4)n_4 , \quad (15e)$$

where $S=s_1+s_0$ and $N=n_0+n_1+n_2+n_3+n_4$. s_i and n_i are the populations of the ith energy levels of the Yb^{3+} ions, $^2F_{7/2}$ and $^2F_{5/2}$, and Ho^{3+} ions, $^5I_8$, $^5I_7$, $^5F_5$, $^5S_2$, $^5F_4$, and $^5F_3$, respectively. S and N are the total concentrations of Yb^{3+} and Ho^{3+} ions, W_p is the pumping rate for absorbing photons from the laser excitation, χ_i $(i=1,2)$ is the energy-transfer coefficient, γ_i $(i=1,2)$ is the back-transfer coefficient, β_0 is the fluorescence-decay rate of the $^2F_{5/2}$ level of Yb^{3+}, β_i $(i=1-5)$ is the fluorescence-decay rate of each Ho^{3+} level as shown in the figure, and κ is the nonradiative-decay rate from $^5F_3$ to $^5S_2$,$^5F_4$.

These equations were solved numerically on a DEC Micro-Vax II microcomputer using a fourth-order Runge-Kutta method in order to find the transient solutions. A δ-function excitation was assumed and the four transfer coefficients were treated as adjustable parameters. The observed fluorescence intensity from each level will be proportional to the population of the level. The time evolution of the fluorescence emissions from the $^2F_{5/2}$ level of Yb^{3+} and the $^5S_2$,$^5F_4$ levels of Ho^{3+} are shown in Fig. 11. The solid and dashed lines represent the computer-generated least-squares fit to the data using the theoretical model described above. The data taken at 12 K were analyzed because the $^5F_3$ emission is too weak to detect at higher temperatures due to the increase in the multiphonon emission rate with temperature, and the Yb^{3+} emission is strongest at 12 K, as shown in Fig. 7. This analysis provides a fit of two sets of data with the same set of adjustable parameters. The best-fit parameters are listed in Table IV and are estimated to be accurate to ±10%. The intensity of the green emission as a function of laser-pump power is found to be almost quadratic, as shown in Fig. 12. This is expected for any two-photon process. Figure 13 shows the excitation spectra for the green up-conversion along with the absorption spectra in the region of the $^5F_5$ state of Ho^{3+}. The excitation spectra have been corrected for variations in laser power and the penetration depth into the sample. This shows a one-to-one correspondence with the positions of the peaks in the absorption spectra.

TABLE IV. Parameters obtained from the rate-equation analyses.

Activator level	Coefficient (cm^3/sec)	Transfer rate (sec^{-1})
	Up-conversion of red pump light at 12 K	
χ_1 (s_0)	2.1×10^{-17}	2.5×10^5
γ_1 (n_1)	3.0×10^{-8}	3.0×10^5
χ_2 (n_1)	5.0×10^{-9}	5.0×10^4
γ_2 (s_0)	5.7×10^{-18}	6.8×10^4
κ	2.0×10^4 sec^{-1}	
	Up-conversion of infrared pump light at 300 K	
χ_1 (n_0)	7.0×10^{-18}	6.3×10^3
γ_1 (s_0)	1.0×10^{-21}	12.0
χ_2 (n_1)	3.1×10^{-8}	1.5×10^5
γ_2 (s_0)	1.4×10^{-17}	1.7×10^5
χ_3 (n_2)	1.0×10^{-7}	1.0×10^5
γ_3 (s_0)	2.0×10^{-17}	2.4×10^5
ϕ_1	1.00 cm^3/sec	
ϕ_2	0.05 cm^3/sec	
τ_1	10 psec	
τ_2	10 psec	

The kinetics leading to the green emission from the $^5S_2$,$^5F_4$ levels after excitation into the inhomogeneously broadened $^2F_{5/2}$ state of the Yb^{3+} ion can be modeled as shown in Fig. 1. The first step in the up-conversion is the energy transfer from Yb^{3+} to Ho^{3+},

$$|\,Yb^{3+}(^2F_{5/2}),Ho^{3+}(^5I_8)\rangle \rightarrow |\,Yb^{3+}(^2F_{7/2}),Ho^{3+}(^5I_6)\rangle .$$

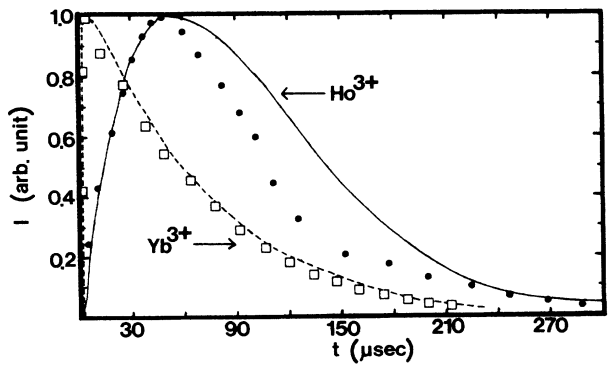

FIG. 11. Decay kinetics of emission from $^2F_{5/2}$ level of Yb^{3+} and $^5S_2$,$^5F_4$ level of Ho^{3+} at 12 K with rate-equation fits.

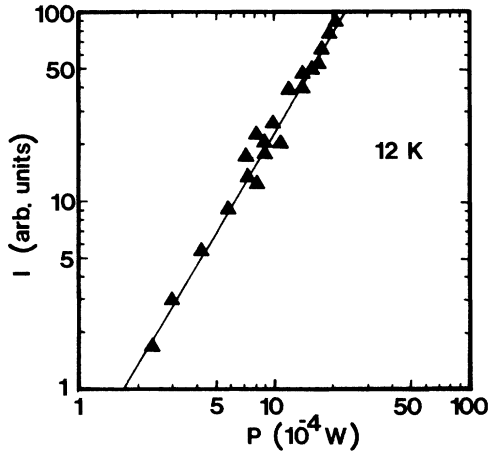

FIG. 12. Power dependence of green up-conversion, obtained by pumping $^5F_5$ and observing green emission from $^5S_2$,$^5F_4$ at 12 K.

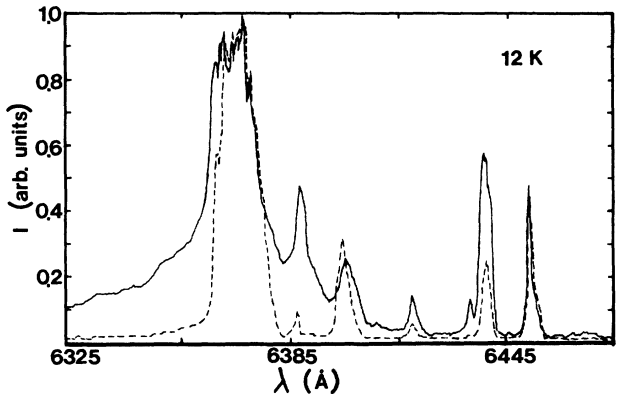

FIG. 13. Excitation spectra for green up-conversion in the region of $^5F_5$ level of Ho^{3+} at 12 K (dashed line) along with absorption spectra in the same region at 12 K (solid line).

This is a nonresonant process and the difference in energy is made up by the emission of phonons. As can be seen from the energy-level diagram, Fig. 1, the energy mismatch is about 1700 cm^{-1}. The phonons in this material have a maximum energy of approximately[41] 450 cm^{-1}; therefore the phonon-assisted energy transfer takes place with the emission of at least four phonons. The back-transfer rate from Ho^{3+} to Yb^{3+} should be smaller than the forward-transfer rate by a factor of[3] $[\exp(\Delta E/k_B T)]^4$, where ΔE is the energy of the phonons absorbed. This difference in rates is approximately 3 orders of magnitude at room temperature. The next step in the total scheme is the resonant cross-relaxation

$$|\,Yb^{3+}(^2F_{5/2}),Ho^{3+}(^5I_6)\rangle \rightarrow |\,Yb^{3+}(^2F_{7/2}),Ho^{3+}(^5S_2,^5F_4)\rangle\ .$$

The third step, which is necessary in order to explain the observed dependence of the green-emission intensity on infrared pump power as discussed below, is also resonant. This process is

$$|\,Yb^{3+}(^2F_{5/2}),Ho^{3+}(^5S_2,^5F_4)\rangle \rightarrow |\,Yb^{3+}(^2F_{7/2}),Ho^{3+}(^3H_6)\rangle\ .$$

In both of these resonant processes, back-transfer cánnot be neglected. The presence of back-transfer was confirmed experimentally by the observation of the emission at 1.0 μm due to Yb^{3+} after pumping the $^5S_2$,$^5F_4$ and $^3H_6$ states of Ho^{3+}. The risetime for the Yb^{3+} emission was measured to be 15 μsec at 12 K.

The rate equations for this model are

$$\frac{ds_1}{dt}=W_p(S-s_1)-\chi_1 s_1(N-n_1-n_2-n_3)+\gamma_1 n_1(S-s_1)-\chi_2 s_1 n_1+\gamma_2 n_2(S-s_1)-\chi_3 s_1 n_2+\gamma_3 n_3(S-s_1)-\beta_0 s_1\ , \tag{16a}$$

$$\frac{dn_1}{dt}=\chi_1 s_1(N-n_1-n_2-n_3)-\gamma_1 n_1(S-s_1)-\chi_2 s_1 n_1+\gamma_2 n_2(S-s_1)-\beta_1 n_1-\phi_1 n_1 p_1\ , \tag{16b}$$

$$\frac{dn_2}{dt}=\chi_2 s_1 n_1-\gamma_2 n_2(S-s_1)-\chi_3 s_1 n_2+\gamma_3 n_3(S-s_1)-\beta_2 n_2-\phi_2 n_2 p_2\ , \tag{16c}$$

$$\frac{dn_3}{dt}=\chi_3 s_1 n_2-\gamma_3 n_3(S-s_1)-\beta_3 n_3\ , \tag{16d}$$

$$\frac{dp_1}{dt}=\phi_1 n_1 p_1+\beta_1 n_1-p_1/\tau_1\ , \tag{16e}$$

$$\frac{dp_2}{dt}=\phi_2 n_2 p_2+\beta_2 n_2-p_2/\tau_2\ , \tag{16f}$$

where the definitions of the parameters are as described following Eqs. (15). Here, s_i and n_i are the populations of the ith energy levels of the Yb^{3+} ions, $^2F_{7/2}$ and $^2F_{5/2}$, and Ho^{3+} ions, $^5I_8$, $^5I_6$, $^5S_2^5F_4$, and $^3H_6$, respectively. Terms representing stimulated-emission transitions from levels n_1 and n_2 are included in the model. Stimulated emission from n_1 occurs at[5,6] 2.9 μm, and p_1 represents the total number of photons at this wavelength in the sample. ϕ_1 represents the stimulated-emission parameter which is related to the stimulated-emission threshold, and τ_1 represents losses in the sample at this wavelength.[43] Stimulated emission from n_2 occurs at[1] 551.5 nm, and p_2, ϕ_2, and τ_2 represent the same parameters for this transition. As shown below, it is necessary to include stimulated emission at 551.5 nm in order to explain the observed power dependence of the green up-conversion and the observed lifetime shortening. The stimulated emission from n_1 must be included because we have determined the threshold for laser action at[5] 2.9 μm to be 80 mJ corresponding to a pumping rate of 4.3×10^{21} photons/sec. This threshold occurs at a considerably lower pumping rate than that used in our spectroscopic measurements (10^{24}–10^{27} photons/sec). Omission of this term will lead to nonphysical values for the energy-transfer coefficients, tending to overestimate the forward-transfer coefficients χ_i.

Figure 14 shows the power dependence of the intensity of the green fluorescence versus the power of the infrared pump laser. The data show the presence of saturation effects since the slope is much less than quadratic, as is usually expected for a two-photon process. At a pumping rate of 4.0×10^{26} photons/sec the slope of the curve shows a significant increase which is due to stimulated emission. The change in slope corresponds to the threshold for this process and is consistent with the onset of the observed lifetime shortening discussed below. This power dependence was modeled using the rate equations given in Eqs. (16). These equations were solved numerically using the same computer procedure described above. A δ-function excitation was assumed and the transfer coefficients χ_2, χ_3, γ_3, and the stimulated-emission parameter ϕ_2 were treated as adjustable parameters. χ_1 can be estimated from the risetime of the 1.2-μm emission and γ_1 was chosen to be approximately 3 orders of magnitude smaller, as discussed earlier. χ_1 was chosen to be 7.0×10^{-18} cm^3/sec, agreeing with earlier estimates,[14,37] and γ_1 was chosen to be 1.0×10^{-21} cm^3/sec. γ_2 can be measured by exciting Ho^{3+} in the $^5S_2$,$^5F_4$ levels and measuring the risetime of the $^2F_{5/2}$ Yb^{3+} emission.

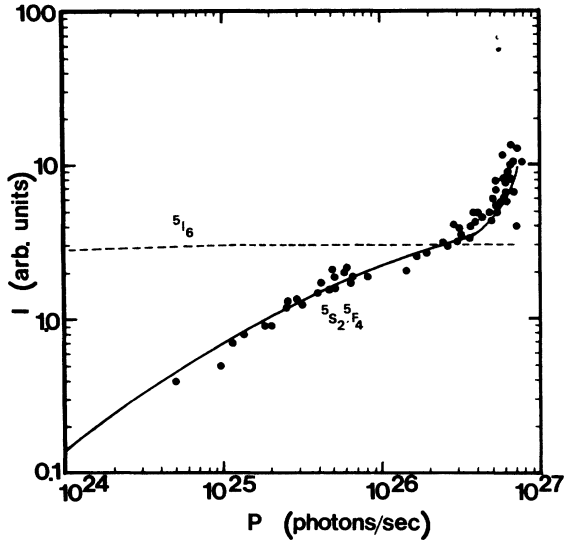

FIG. 14. Power dependence of green up-conversion, obtained by pumping $^2F_{5/2}$ level of Yb^{3+} at room temperature.

From these measurements γ_2 was calculated to be 1.4×10^{-17} cm^3/sec. The measured fluorescence-decay rates were used for the transition rates. τ_1 and τ_2 were chosen to be 10 psec, the time it takes light to pass through the sample.[42] ϕ_1 was chosen to agree with the threshold for the 2.9-μm laser action using the equation

$$n_1=(\tau_1\phi_1)^{-1} . \tag{17}$$

This is obtained by defining the threshold as when the gain terms equals the loss term in Eq. (16e). The resulting best fit to the data is shown as a solid line in Fig. 14. The values for the adjustable parameters obtained from this fit are listed in Table IV and estimated to have an accuracy of $\pm10\%$.

The peak intensities of green emission plotted in Fig. 14 and in the theoretical fit were chosen at the peak of the rise in the number of photons, p_2, in the sample. This time was about 1.5 μsec for pump powers below the threshold for stimulated emission in the green transition and became shorter above the threshold, eventually becoming limited by experimental resolution. The time evolution of the green emission below this threshold was also calculated from the rate equations and is shown along with the experimentally measured data in Fig. 15.

Under the condition of low-power infrared excitation the lifetime of the green transition is measured to be approximately 47 μsec. When the excitation power is increased to the threshold value of 4.0×10^{26} photons/sec and above, the shape of the decay curve abruptly changes. The short-time emission decays much faster than at low excitation powers, and the long-time decay is the same as for the low-power excitation. The $1/e$ value of the decay curve is plotted as a function of pump power in Fig. 16. The general shape of these data is similar to that reported in Refs. 42 and 43 and shows a definite excitation threshold. The fact that the intensity of the green emission increases instead of decreases above this threshold value confirms that we are observing a gain and not a loss mechanism. The increase in intensity is a result of the stimulated emission which causes the emission of photons at earlier times (lifetime shortening), thereby inhibiting the third energy-transfer step.

The model presented here has one more energy-transfer step than is necessary to explain the population of the $^5S_2,^5F_4$ states by the up-conversion mechanism. The additional energy-transfer process to the $^3H_6$ level must be included in order to explain the observed power dependence shown in Fig. 14. This level acts as a "sink" for the excitation since population can accumulate in this level or decay into levels other than n_1 or n_2 without being recycled into these metastable levels on the time scale of the green emission. Without this additional energy level the green-emission intensity dependence on pump power cannot become sublinear.[44] In this case the model is essentially a closed system, on the time scale of the experiment, because the decay times are much longer than the observed risetimes at which the data were taken. The saturation behavior of the population of n_2 would, at

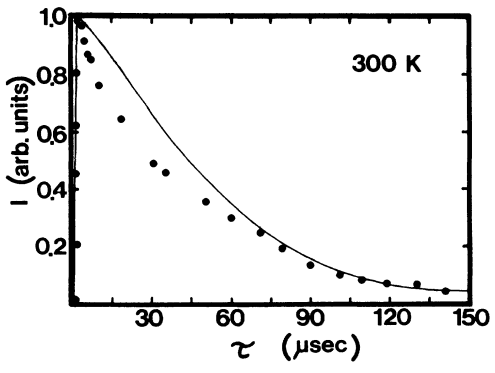

FIG. 15. $^5S_2,^5F_4$ decay kinetics with rate-equation fit.

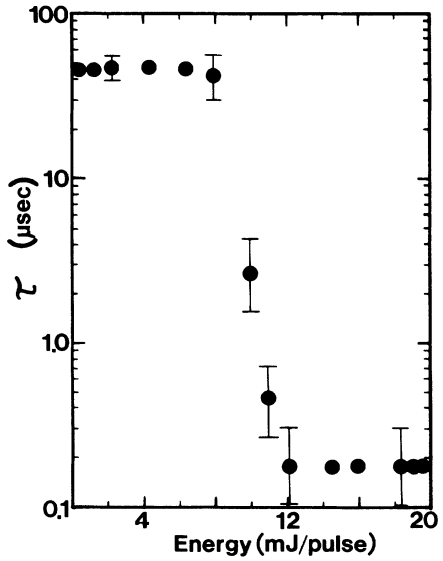

FIG. 16. Decay time of $^5S_2,^5F_4$ at room temperature as a function of excitation power showing lifetime shortening.

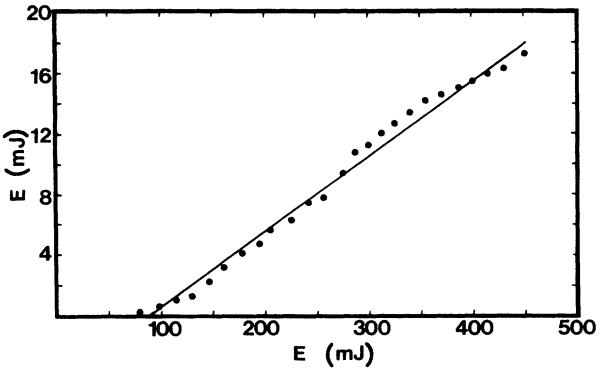

FIG. 17. Conversion efficiency of 2.9-μm laser output, pumping with the 1.047-μm output of a Nd:YLF laser.

best, decrease from a quadratic to a linear dependence on pump power, and the slope could not become any smaller without this additional level.

Figure 17 shows the laser output energy at 2.9 μm as a function of the energy input into the crystal at room temperature. Laser action was achieved by end-pumping the laser rod with a Nd:YLF laser constructed in-house. The pump laser had a wavelength of 1.047 μm and a pulse width of 60 μsec. The YLF laser was operated in the long-pulse regime with no mode-selective elements and a 30% output coupler. Output energies up to 750 mJ are obtainable from the pump laser. The 2.9-μm laser cavity consisted of a flat high reflector (greater than 99% reflecting at 2.9 μm) and a flat output coupler (approximately 90% reflecting at 2.9 μm), separated by 5 cm. An energy-conversion efficiency of 15% is obtained with a slope efficiency of 4.5% and a fractional pump light absorption in the rod of 0.33 times the incident energy on the laser rod. The threshold for 2.9-μm lasing action was found to be 80 mJ of incident pump energy. Antipenko *et al.*[6] have reported a conversion efficiency of 7.5% using the 1.061-μm emission from a Nd:GSGG (GSGG denotes gadolinium scandium gallium garnet) laser as a pumping source. The increased efficiency obtained here is a result of the larger Yb^{3+} absorption coefficient at 1.047 μm. Similar results were obtained using an 80% reflecting output coupler, suggesting that the threshold and extraction efficiency are dominated by scattering losses in the rod.

The saturation of the $^5I_6$ population mentioned earlier in connection with the rate equations is not evident in these results. This is because the pumping power is not large enough for the second energy-transfer process in Fig. 1 to become dominant over the first energy-transfer process.

VI. DISCUSSION

To interpret the data presented above, a theoretical estimate must be obtained for the magnitude and temperature dependence of D, and relationships between the various energy-transfer parameters must be established. The physical meaning of the stimulated-emission parameter must also be determined.

A theoretical calculation of the magnitude of the diffusion constant is difficult since the details of the exciton band shape are not known. A rough theoretical estimate for D can be obtained by considering the rate of energy transfer between two Yb^{3+} ions. Assuming that the interaction mechanism between Yb^{3+} ions is dipole-dipole in nature, the energy-transfer rate between two ions separated by a distance R is[28,31]

$$P(R)=1/\tau(R_0/R)^6 , \tag{18}$$

where R_0 is again the critical interaction distance. For multistep energy migration, the diffusion coefficient can be expressed in terms of the interaction rate between ions as[45]

$$D=\tfrac{1}{6}\int_0^\infty R^2P(R)\rho(R)dR , \tag{19}$$

where $\rho(R)$ is the probability of finding an ion at a distance R from the ion at the origin, and for a random distribution is given by[45]

$$\rho(R)=4\pi N_s R^2\exp(-4\pi N_s R^3/3) . \tag{20}$$

With these expressions the diffusion constant becomes

$$D=\tfrac{2}{3}(\pi N_s R_0^6/\tau_s)\int_d^\infty R^{-2}\exp(-4\pi N_s R^3/3)dR . \tag{21}$$

Note that the lower limit of the integral is taken to be the smallest distance between Yb^{3+} ions. Using the value of $d=2.7$ Å along with the concentration and intrinsic decay rate of Yb^{3+} ions, $N_s=1.2\times10^{22}$ cm^{-3} and $\tau_s^{-1}=555$ sec^{-1}, the integral in Eq. (21) can be evaluated numerically to give a value of 1.23×10^6, yielding the result

$$D=1.7\times10^{31}R_0^6 . \tag{22}$$

Using the values of D calculated from the Chow-Powell theory, the value of R_0 can be calculated. At 12 K, R_0 equals to 10.3 Å, while at 250 K, R_0 equals 13.8 Å. These values are listed in Table III.

The temperature dependence of D, shown in Fig. 9, can give some qualitative information about the exciton motion in the Yb^{3+} system. Figure 9 shows that D increases with temperature, which implies that the exciton motion is a thermally assisted incoherent process. This can be represented by

$$D(T)=D(0)+B\exp(-\Delta E/k_BT) , \tag{23}$$

where $D(0)$ is the diffusion constant at zero temperature, ΔE is the activation energy of the thermally assisted process, and k_B is Boltzmann's constant. $D(0)$ is the resonant contribution to the diffusion, and B is the parameter describing the nonresonant contribution to the diffusion. The best-fit parameters obtained from a least-squares-fitting procedure are listed in Table III.

As shown previously, the results of the Inokuti-Hirayama analysis of the Ho^{3+}–Yb^{3+} energy transfer and the Chow-Powell analysis of the Yb^{3+}–Ho^{3+} energy transfer are related in terms of transfer and back-transfer processes. The differences in the magnitudes of the energy-transfer rates are associated with the changes in the role of the sensitizer and activator ions, which change the spectral overlap due to the energy shift between absorption and emission transitions. Because most of the

energy-transfer processes take place with the activator ion initially in an excited state, it is not possible to calculate the overlap integral since there is no excited-state absorption information available on this material. For this reason it is not possible to correlate the transfer rates with the spectral data.

The computer models used to explain the two different types of up-conversion also provide values for the energy-transfer rates. In order to correlate the transfer coefficients with the transfer rates obtained from the two energy-transfer theories, it is necessary to multiply the transfer coefficients by the concentration of the initial activator energy level.[17] The appropriate levels for each transfer coefficient are listed in Table IV. Because the pumping rates used in these experiments do not deplete the ground states to any appreciable extent, the excited-state populations of Ho^{3+} are quite low compared to the ground-state populations. Therefore, in order for the forward- and back-transfer rates to be equal for the resonant transitions, the transfer coefficients must be several orders of magnitude different. In addition, the transfer rates for two different resonant transitions may be equal, but the corresponding transfer coefficients may not be equal. Previous studies[3,11,12,14,37] using similar rate-equation models have assumed that the resonant transfer coefficients are equal, instead of the resonant transfer rates, as done here.

The risetimes of Yb^{3+} emission after pumping the $^5Y_5$ and $^5S_2$,$^5F_4$ states of Ho^{3+} are 4 and 15 μsec at 12 K, respectively, in agreement with the difference in the interaction strengths. The risetime of the $^5S_2$,$^5F_4$ emission after pumping the $^5F_5$ level of Ho^{3+} is 48 μsec. From these results and Eq. (14) the rate of the second transfer process in Fig. 10 can be calculated to be approximately 2.0×10^4 sec^{-1}. This is in good agreement with our rate-equation results listed in Table IV (5.0×10^4 sec^{-1}). The nearest-neighbor energy-transfer rates predicted from the Inokuti-Hirayama theory are smaller than the rates predicted from the rate-equation models. This is a result of the neglect of back-transfer. The energy-transfer rate predicted for the Yb^{3+}-Ho^{3+} interaction from the Chow-Powell theory is also smaller than the rate predicted from just the χ_2 term in Eqs. (16). Both energy-transfer models suffer as a result of neglecting the back-transfer of excitation energy, whereas the rate-equation approach properly takes back-transfer into account at the expense of using time-independent transfer rates. Neglecting back-transfer causes the sensitizer-activator strength to be underestimated.

The rate-equation models were used to fit the time dependence of the up-conversion emission. The results are shown as solid and dashed lines in Figs. 11 and 15. The theoretical calculations agree well with the risetime and asymptotic ($t\rightarrow\infty$) behaviors of the data, but the fits are poor in the the time region just after the maximum population of the level has been reached. The reason for this is that the transfer coefficients used in the rate equations were time independent, and hence the only time dependence in the transfer rate was contained in the concentration of acceptor ions in the specific level involved. The decay kinetics shown in Figs. 5 and 8 can be interpreted accurately by models with time-dependent transfer rates, such as those of Inokuti-Hirayama and Chow-Powell. These time-dependent transfer rates manifest themselves predominantly in the early portions of the decay, where the constant transfer coefficients give a poor fit, leading to nonexponential decays. The parameters obtained from these models should be taken as approximate average values of the real time-dependent values of the energy-transfer rates.

The stimulated-emission parameters used in this model of the infrared up-conversion are related to the threshold for stimulated emission. The spontaneous-emission term in Eq. (16f), $\alpha_2 n_2$, acts as a feeding mechanism for the total number of photons of a particular wavelength in the sample. The other two terms in this equation are competitive in nature. When the gain term $\phi_2 n_2 p_2$ equals the loss term p_2/τ_2, then threshold has been reached. Substitution of the values from Table IV into Eq. (17) gives a value for n_2 of 2.0×10^{12} cm^{-3}. This implies a threshold of 1.5×10^4 W/cm^3 for direct pumping of this level, and consequently a higher value for the threshold for infrared excitation of Yb^{3+}. For a pure two-photon process without losses, the threshold would be 3.0×10^4 W/cm^3. However, losses in this system are not negligible, as discussed earlier in connection with the saturation behavior and inclusion of a third energy-transfer process. As a result, the actual threshold for stimulated emission in the green after infrared excitation would be still higher. Experimentally the threshold was observed to be 75 MW/cm^3 for infrared excitation. The simplified model used to describe the stimulated emission is largely responsible for the discrepancy in threshold values.[43]

At the high pumping powers used here, the efficiency of the infrared excitation of the green emission is not as high as at lower pump powers. This is reflected in the saturation of the power dependence shown in Fig. 14, and in the population of n_2 obtained from the computer fits. This is a result of the third transfer process becoming more effective at higher pump powers.[4,44] The saturation of the population of the $^5I_6$ level shown in Fig. 14 is also evident in the laser output at 2.9 μm when large pump powers are used.[4] This is a result of the difference in transfer rates obtained from Eqs. (16), $\chi_1(n_0)$ and $\chi_2(n_1)$. Because the first transfer from Yb^{3+} is nonresonant while the second one is resonant, the population of $^5I_6$ starts to level off at a specific pump power,[4] ≈1 kW/cm^3, as a result of the second transfer becoming more efficient at this power level. The saturation of $^5I_6$ has been observed[44] at a pump energy of 0.6 J/cm^3 or 2.7×10^{23} photons/sec for a crystal containing 0.5 at.% Ho^{3+}. This is slightly larger than the value calculated here due to the difference in concentration of Ho^{3+} ions.

Another mechanism for decreasing the 2.9-μm laser output at high pump powers is population of the terminal level of the 2.9-μm emission,[44] $^5I_7$. The $^5I_7$ state is metastable, having a lifetime of 9 msec, so that population of this level decreases the inversion for the 2.9-μm stimulated-emission transition. There are two effective mechanisms for populating the $^5I_7$ level after 1.0-μm pumping. The first, which is the dominant process at low pump powers, is nonradiative decay from $^5I_6$ to $^5I_7$. The

second process, which only becomes effective at high pump powers, is a result of two cross-relaxation processes after the third transfer from Yb^{3+} to Ho^{3+}. The third transfer populates $^3H_6$ and then nonradiative decay to $^5G_4$ occurs.[44] The first cross-relaxation is

$$|\,Ho^{3+}(^5G_4), Yb^{3+}(^2F_{7/2})\rangle \rightarrow |\,Ho^{3+}(^5F_5), Yb^{3+}(^2F_{5/2})\rangle\ .$$

The second cross-relaxation is

$$|\,Ho^{3+}(^5F_5), Yb^{3+}(^2F_{7/2})\rangle \rightarrow |\,Ho^{3+}(^5I_7), Yb^{3+}(^2F_{5/2})\rangle\ .$$

Both are resonant processes. The second cross-relaxation is exactly the first step in the up-conversion of 640-nm radiation into 551.5-nm radiation, Fig. 10. This is the connection between the two up-conversion models. This process is only effective in populating $^5I_7$ at high pump powers, because the third transfer from Yb^{3+} to Ho^{3+} is only effective at high pump powers. A result of the increase in population of the $^5I_7$ level is an increase in the output at 2.0 μm. This mechanism should become effective in populating $^5I_7$ at the pump powers at which it becomes necessary to include the third transfer from Yb^{3+} to Ho^{3+}.

VII. CONCLUSIONS

The characteristics of the interaction between the rare-earth ions in $BaYb_2F_8$:Ho^{3+} crystals in several energy levels has been calculated and it has been shown that the interaction is electric-dipole–dipole. The coupling between Ho^{3+} and Yb^{3+} ions is greater for the $^5F_5$ state of Ho^{3+} than it is for the $^5S_2$, $^5F_4$ states. The multistep migration of energy among Yb^{3+} ions is much stronger than the Yb^{3+}-Ho^{3+} interaction, having a mean free path of 85 Å at 250 K. This justifies the treatment of the Yb^{3+} ions as always being able to transfer their energy to nearest-neighbor Ho^{3+} ions since energy migrates from one Yb^{3+} to another until a Ho^{3+} ion is close enough for the transfer from Yb^{3+} to Ho^{3+} to take place.

Multiple energy-transfer processes were shown to lead to up-conversion, switching of lasing channels, and saturation. An important conclusion is that a model with just two transfers from Yb^{3+} to Ho^{3+} is insufficient to explain the observed data.[4,44] Energy transfer from Yb^{3+} to Ho^{3+} in the $^5s_2$, $^5F_4$ states resulting in excitation of the Ho^{3+} ion to the $^3H_6$ state must be included for the high pumping powers used here. Therefore, as the pump power is increased the efficiency of the short-wavelength stimulated emission, 0.55 μm, increases, while the efficiency of the longer-wavelength stimulated emission, 2.9 μm, decreases. At still larger pump powers the third energy transfer causes the 0.55μm stimulated emission to be less efficient.

The laser-performance results for the 2.9-μm laser action have shown that the efficiency of the laser action can be significantly increased by pumping into a Yb^{3+} spectral region with a larger absorption coefficient. Since the Yb^{3+} absorption peaks at approximately 960 nm at room temperature, diode pumping should be an effective method of achieving improved efficiency in the 2.9-μm laser action. However, as we have shown in connection with the rate-equation analysis, the efficiency of this laser channel is limited by saturation effects, and therefore the very large difference in the absorption coefficient at 960 nm as opposed to 1047 nm (greater than an order of magnitude) may not be reflected in the increased efficiency of the 2.9-μm laser action.

ACKNOWLEDGMENTS

This research was sponsored by the U.S. Army Research Office. One of us (G.D.G.) was supported in part by the Office of Naval Research, U.S. Department of Defense.

[1]L. F. Johnson and H. J. Guggenheim, Appl. Phys. Lett. **19**, 44 (1971).
[2]S. A. Pollack, D. B. Chang, and N. L. Moise, J. Appl. Phys. **60**, 4077 (1986).
[3]L. F. Johnson, H. J. Guggenheim, T. C. Rich, and F. W. Ostermayer, J. Appl. Phys. **43**, 1125 (1972).
[4]B. M. Antipenko, I. V. Vorykhalov, B. V. Sinitsyn, and T. V. Uvarova, Kvantovaya Elektron. (Moscow) **7**, 197 (1980) [Sov. J. Quantum Electron. **10**, 114 (1980)].
[5]P. Lacovara, G. D. Gilliland, and L. Esterowitz, Proc. SPIE (to be published).
[6]B. M. Antipenko, B. V. Sinitsyn, and T. V. Uvarova, Kvantovaya Elektron. (Moscow) **7**, 2019 (1980) [Sov. J. Quantum Electron. **10**, 116B (1980)].
[7]F. Auzel, Phys. Rev. B **13**, 2809 (1976).
[8]F. Auzel, Proc. IEEE **61**, 758 (1973).
[9]R. A. Hewes and J. F. Sarver, Phys. Rev. **182**, 427 (1969).
[10]R. A. Hewes, J. Lumin. **1,2**, 778 (1970).
[11]F. W. Ostermayer, Jr. and L. G. Van Uitert, Phys. Rev. B **1**, 4208 (1970).
[12]F. W. Ostermayer, Jr., J. P. van der Ziel, H. M. Marcos, L. G. Van Uitert, and J. E. Geusic, Phys. Rev. B **3**, 2698 (1972).
[13]L. F. Johnson, J. E. Geusic, H. J. Guggenheim, T. Kushida, S. Singh, and L. G. Van Uitert, Appl. Phys. Lett. **15**, 48 (1969).
[14]R. K. Watts, J. Chem. Phys. **53**, 3552 (1970).
[15]D. C. Yeh, W. A. Sibley, M. Suscavage, and M. G. Drexhage, J. Appl. Phys. **62**, 266 (1987).
[16]T. C. Rich and D. A. Pinnow, J. Appl. Phys. **43**, 2357 (1972).
[17]J. C. Wright, Top. Appl. Phys. **15**, 239 (1976).
[18]J. D. Kingsley, J. Appl. Phys. **41**, 175 (1970).
[19]L. F. Johnson and H. J. Guggenheim, Appl. Phys. Lett. **23**, 96 (1973).
[20]B. R. Judd, Phys. Rev. **127**, 750 (1962).
[21]G. S. Ofelt, J. Chem. Phys. **37**, 511 (1962).
[22]M. J. Weber, B. H. Matsinger, V. L. Donlan, and G. T. Surratt, J. Chem. Phys. **57**, 562 (1972).

[23]A. A. Kaminskii, B. P. Sobolev, and T. V. Uvarova, Phys. Status Solidi A **78**, K13 (1983).
[24]L. F. Johnson and H. J. Guggenheim, IEEE J. Quantum Electron. **QE-10**, 442 (1974).
[25]O. E. Izotova and V. B. Aleksandrov, Dokl. Akad. Nauk SSSR **192**, 1037 (1970) [Sov. Phys.—Dokl. **15**, 525 (1970)].
[26]*Landolt-Börnstein, New Series, Crystal Structure Data of Inorganic Compounds, Key Elements: F, Cl, Br, I* (Springer-Verlag, New York, 1973), Vol. III/7a, p. 170.
[27]W. T. Carnall, P. R. Fields, and K. Rajank, J. Chem. Phys. **49**, 4424 (1968).
[28]M. Inokuti and F. Hirayama, J. Chem. Phys. **43**, 1978 (1965).
[29]H. C. Chow and R. C. Powell, Phys. Rev. B **21**, 3785 (1980).
[30]D. L. Dexter, J. Chem. Phys. **21**, 836 (1953).
[31]T. Forster, Ann. Phys. (Leipzig) **2**, 55 (1948); Z. Naturforsch. **4a**, 321 (1949); Discuss. Faraday Soc. **27**, 7 (1959).
[32]M. Yokota and O. Tanimoto, J. Phys. Soc. Jpn. **22**, 779 (1967).
[33]C. M. Lawson, E. E. Freed, and R. C. Powell, J. Chem. Phys. **76**, 4171 (1982).
[34]R. K. Watts and H. J. Richter, Phys. Rev. B **6**, 1584 (1972).
[35]M. J. Weber, Phys. Rev. B **4**, 2932 (1971).
[36]B. M. Antipenko, Opt. Spektrosk. **56**, 72 (1984) [Opt. Spectrosc. (USSR) **56**, 44 (1984)].
[37]R. K. Watts and W. C. Holton, Solid State Commun. **9**, 137 (1971).
[38]H. J. Guggenheim and L. F. Johnson, Appl. Phys. Lett. **15**, 51 (1969).
[39]G. F. De Sa, P. A. Santa Cruz, and F. Auzel, J. Lumin. **31,32**, 693 (1984).
[40]R. C. Powell and G. Blasse, in *Structure and Bonding,* edited by J. D. Dunitz, J. B. Goodenough, P. Hemmerich, J. A. Ibers, C. K. Jorgensen, J. B. Neilands, D. Reinen, and R. J. P. Williams (Springer, Berlin, 1980), Vol. 42, p. 43; M. D. Shinn and W. A. Sibley, Phys. Rev. B **29**, 3834 (1984).
[41]B. M. Antipenko, S. P. Voronin, Sh. N. Gifeisman, R. V. Dubravyanu, Yu. E. Perlin, T. A. Privalova, and O. B. Raba, Opt. Spectrosk. **58**, 1270 (1985) [Opt. Spectrosc. (USSR) **58**, 780 (1985)].
[42]G. M. Loiacono, M. F. Shone, G. Mizell, R. C. Powell, G. J. Quarles, and B. Elouadi, Appl. Phys. Lett. **48**, 622 (1986).
[43]M. L. Kliewer, A. B. Suchocki, and R. C. Powell (unpublished).
[44]B. M. Antipenko, Pis'ma Zh. Tekh. Fiz. **6**, 968 (1980) [Sov. Tech. Phys. Lett. **6**, 417 (1980)].
[45]S. Chandrasekhar, Rev. Mod. Phys. **15**, 1 (1943).